Available online at www.sciencedirect.com

ScienceDirect

Journal of Electrocardiology 49 (2016) 569 – 578

JOURNAL OF Electrocardiology

www.jecgonline.com

Transmural, interventricular, apicobasal and anteroposterior action potential duration gradients are all essential to the genesis of the concordant and realistic T wave: A whole-heart model study ☆

Yi Zheng, PhD, [a] Daming Wei, PhD, [b,*] Xin Zhu, PhD, [a] Wenxi Chen, PhD, [a] Koji Fukuda, MD, PhD, [b] Hiroaki Shimokawa, MD, PhD [b]

[a] *Biomedical Information Technology Lab, the University of Aizu, Tsuruga, Ikki-machi, Aizu-Wakamatsu, Fukushima, Japan*

[b] *Department of Cardiovascular Medicine, Tohoku University Graduate School of Medicine, Seiryo-Machi 1-1, Aoba-ku, Sendai, Miyagi, Japan*

Abstract

Background: It has been reported that ventricular repolarization dispersion resulting from transmural, apicobasal and interventricular action potential duration (APD) gradients makes the T wave concordant with the QRS complex.

Method and results: A whole-heart model integrating transmural, apicobasal, interventricular and anteroposterior APD gradients was used, and the corresponding electrocardiograms were simulated to study the influence of these APD gradients on the T-wave amplitudes. The simulation results showed that changing a single APD gradient (e.g., interventricular APD gradient alone) only made substantial changes to the T-wave amplitudes in a limited number of leads and was not able to generate T waves with amplitudes comparable with clinical findings in all leads. A combination of transmural, apicobasal and interventricular APD gradients could simulate T waves with amplitudes similar to clinical values in the limb leads only. Adding the anteroposterior APD gradient into the model greatly improved the consistency between the simulated T-wave amplitudes and the clinical values.

Conclusion: The simulation results support that the transmural, apicobasal, interventricular and the anteroposterior APD gradient are all essential to the genesis of the clinical T wave.

Keywords: Electrocardiogram; T wave; Action potential duration gradient; Whole-heart model; Computer simulation

Introduction

It is known that the T wave results from the spatial potential differences because of the ventricular action potential (AP) repolarization dispersion [1]. Because the repolarization moment is the sum of AP duration (APD) and activation moment [2], the repolarization dispersion can be decomposed into the APD dispersion and the depolarization dispersion [3]. According to Abildskov et al. [4], these two dispersions can be theoretically reflected in a primary and secondary T wave, respectively.

The polarity of the secondary T wave is opposite to the QRS complex because the former reflects the downstroke of the AP and the latter represents the upstroke. Consequently the primary T wave is the major component of the realistic T wave that makes the T wave concordant with the QRS complex. Thus the corresponding APD dispersion is recognized as the principal contributor to the T-wave concordance [5]. Many studies have shown that there are different types of electrophysiological heterogeneities (APD dispersion) existing in the ventricles, such as the apicobasal APD gradient [6], the transmural APD gradient [7], the left–right ventricular APD heterogeneity [8–9] and the anteroposterior APD heterogeneity [10].

Unlike the P wave and the QRS complex [11], the source and derivation of the T wave are still controversial [2,12–13]. Various previous studies claimed that the APD (or repolarization) gradients in not all the four anatomic axes mentioned above or even one axis was sufficient to explain the concordant T wave in realistic electrocardiograms (ECG), e.g., the apicobasal axis [14] or the transmural axis [15–17]. Some studies emphasized that the apicobasal axis was superior to the transmural axis [18] or vice versa [19–20]. After investigating the effects of three

Abbreviations: AP, Action Potential; APD, Action Potential Duration; ARI, Activation Recovery Interval; LAO, Left Anterior Oblique; LV, Left Ventricle; RV, Right Ventricle.

☆ This work is supported in part by Japan Society for the Promotion of Science under the Grants-In-Aid for Scientific Research (**No.** 24500369).

* Corresponding author at: Department of Cardiovascular Medicine, Tohoku University Graduate School of Medicine, Seiryo-Machi 1-1, Aoba-ku, Sendai, 980-8574, Japan

E-mail address: daming.wei@ekgtechnol.com

http://dx.doi.org/10.1016/j.jelectrocard.2016.03.010

APD gradients on the T-wave polarity in simulations, Weiss et al. suggested that interventricular APD changes were necessary to reproduce the positive T wave [21], contradicting the conclusion of their consequent study [22]. Unlike the other three APD gradients, the contribution of the anteroposterior APD gradient to the T-wave genesis has been rarely investigated.

Since there are four APD gradients identified in the human heart, it is almost logical that the primary T wave is the electrocardiographical result of all the APD gradients in four anatomic axes. Although animal experiments suggested that repolarization dispersions in all anatomic axes contributed to the T wave [23] and simulations in a rabbit heart model [24] showed that a combination of APD gradients in four axes could generate the most realistic potential distributions, whether all APD gradients are needed to generate a realistic T wave has not been validated in a human heart model.

In this study, we investigated the effect of APD gradients in the four anatomic axes on primary T wave in a human whole-heart model, with a particular focus on how the anteroposterior APD gradient affected the T-wave amplitudes and its role in simulating T-wave amplitudes that were similar to the clinical findings [25].

Method

The whole-heart model

Simulations were carried out in the Wei–Harumi whole-heart model [26]. The heart model is built in an inclined 3-D coordinate system with equal axial angles of 60° [26]. The heart is divided by parallel planes along each of the three axes. The intersection points that coincide with the heart muscle are elements of the heart model and are referred to as "model cells" categorized into several model cell types. Each type can be characterized by assigning the respective action potential, pacing, automaticity and conduction. This model has an endocardium–epicardium rotating fiber orientation. The anisotropic excitation propagation of the model cells (using an anisotropy ratio of 2:1 [27]) complies with Huygens' principle, in which every model cell in the activation wave front represents a source of secondary wave fronts. The range of propagation around each exciting model cell is an ellipsoid-shaped region. Each neighboring model cell within the ellipsoid can either be activated during its excitable period, or be unaffected. The model settings were adjusted to locate the PR interval within the physiological range. The His–Purkinje system was integrated into the model by setting the types of certain model cells as either His or Purkinje model cells. The positions of these model cells were carefully selected and adjusted so that the simulations of normal heart propagations were consistent with the classical data of Durrer et al. [11] and the QRS complex manifested a clinically normal morphology. The reliability of this model in cardiac electrophysiological researches has been proven by many previous studies [28–30].

The action potential

For simplicity, each ventricular model cell shared identical morphologies of phase 0, 1 and 3 of the AP, as well as the potential of the plateau phase. The only difference between them was the duration of the plateau phase: the APD variations were realized by assigning different time spans to the plateau phase [26]. Two typical AP morphologies are shown in the right image of Fig. 1A.

The action potential duration gradient in the transmural axis

In the transmural axis, the ventricles were layered from the epicardium to the endocardium. The thickness of each layer was 1.5 mm. The left image in Fig. 1A shows the layered structure of a cross section through the ventricles. The transmural APD dispersion was realized by assigning different APDs to the corresponding layers.

According to clinical measurements by Taggart et al. [7], the transmural APD increased from the epicardium to the endocardium with an APD gradient of approximately 1 ms/mm. In this study, we assumed that the transmural APD increased linearly from the epicardium to the endocardium with an APD gradient of 1.33 ms/mm to compensate the transmural activation time gradient for difference from the clinical value [7]. The right image of Fig. 1A displays the morphologies of the epicardial and endocardial action potential.

The action potential duration gradients in other axes

The heart was divided into the right and left ventricle (RV and LV, respectively) along the septum, as shown in Fig. 1B (taken from a left anterior oblique (LAO) view). For simplicity, the interventricular APD dispersion was represented by a specific APD difference between the two ventricles.

The ventricles were sliced along the apicobasal axis, as shown in Fig. 1C (again from an LAO view). The apicobasal APD increment was proportional to the sequence number of the corresponding slice. The thickness of each layer was also 1.5 mm.

The right image of Fig. 1D displays the location of the heart inside the torso from a lateral view. The left image is a close-up of the ventricles, divided into anterior and posterior parts by a frontal plane. Like the interventricular APD gradient, the anteroposterior APD dispersion was represented by a specific APD difference between the anterior and posterior areas.

The action potential durations of different model cells

The APD of one model cell was determined by Eq. (1):

$$\begin{aligned} APD = {} & APD_{base} + LayerNum_T \cdot 1.5 \cdot Gradient_T \\ & + LayerNum_{AB} \cdot 1.5 \cdot Gradient_{AB}, \\ & + IV \cdot Gradient_{IV} + AP \cdot Gradient_{AP} \end{aligned} \tag{1}$$

where APD_{base} is the predefined baseline APD (a constant in this study), $LayerNum_T$ is the sequence number of the model cell in the transmural axis (see Fig. 1A for the transmural sequence), $LayerNum_{AB}$ is the sequence number of the model cell in the apicobasal axis (see Fig. 1C for the apicobasal sequence). Because the thickness of one layer is 1.5 mm, both sequence numbers are multiplied by 1.5. IV represents the ventricle that the model cell belongs to ($IV = 1$ for the LV, $IV = 0$ for the RV), and AP is the indicator of the location in anteroposterior direction ($AP = 1$ if the model cell is in the posterior area, $AP = 0$ if the model cell is in the anterior area). $Gradient_T$, $Gradient_{AB}$, $Gradient_{IV}$ and $Gradient_{AP}$ are the transmural, apicobasal, interventricular and anteroposterior APD gradients, respectively.

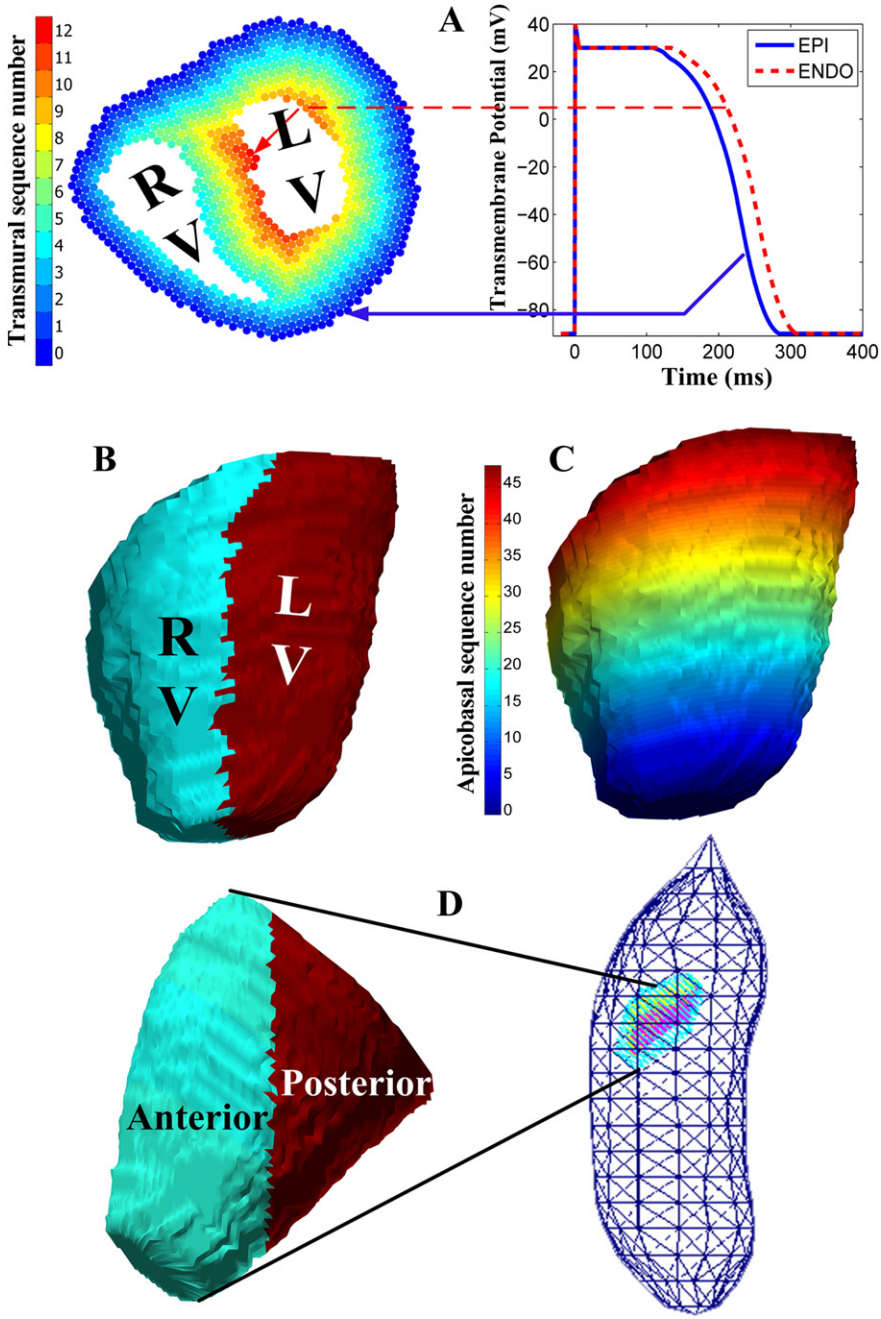

Fig. 1. Schematics of APD gradients in different axes, atria are not shown. (A): A cross section in the left image shows the layered structure for the transmural APD gradient, and each model cell's color indicates its transmural sequence number ($LayerNum_T$ in the Eq. (1)). The right image shows two representative AP morphologies of the epicardial and endocardial model cells. The red-dashed waveform is the action potential of an endocardial model cell, and the blue waveform is the action potential of an epicardial model cell with a shorter plateau phase. The corresponding arrows indicate their locations in the heart. (B): Division of the left and right ventricles. (C): Layer sequence number ($LayerNum_{AB}$ in the Eq. (1)) of the model cells in the apicobasal axis. (D): Division of the anterior and posterior ventricles and the position of the heart inside a torso. Key: RV = right ventricle, LV = left ventricle.

Because homogeneous APD lengthening in the entire ventricular volume only results in elongation of the ST segment rather than T-wave variations [17], the absolute APD value is not as important as the APD dispersion in the genesis of the positive T wave. In other words, the baseline APD can be an arbitrary value. In this study, we set the APD_{base} to 260 ms.

Models with different APD gradients

Table 1 shows the APD gradient settings for five different models. The unit used for the transmural and apicobasal APD gradients was ms/mm, and the unit used for the interventricular and anteroposterior APD dispersions was ms. Model 1 was a model with an homogeneous APD. Model 2 had a transmural APD gradient of 1.33 ms/mm. Based on Model 2, we constructed three models having APD gradients in the other three axes: Model 3 had an apicobasal APD gradient ranging from 0.033 to 0.2 ms/mm; Model 4 had an interventricular APD gradient ranging from −30 to −5 ms; and Model 5 had an anteroposterior APD gradient ranging from 5 to 30 ms.

Table 1
The gradient settings of models.

Model	$Gradient_T$*	$Gradient_{AB}$*	$Gradient_{IV}$**	$Gradient_{AP}$**
1	0	0	0	0
2	1.33	0	0	0
3	1.33	0.033–0.20	0	0
4	1.33	0	−30 – −5	0
5	1.33	0	0	5–30

* Unit is ms/mm.
** Unit is ms.

The action potential gradients and electric cardiac source

The process of depolarization and repolarization throughout the heart is accompanied by the electric current in the intracellular and extracellular spaces, resulting in electric cardiac sources. In this study, the electric cardiac source was represented by the current density, interpreted as the current dipole moment per model cell volume, called the cell dipole [26]. It is mathematically described by:

$$J_i = -D_i \nabla \Phi_i, \tag{2}$$

where J_i is the cell dipole, D_i is the intracellular conductivity tensor, ∇ is the spatial gradient operator and Φ_i is the intracellular potential, which can be derived from the transmembrane potentials.

Surface ECG potentials

The heart model was deployed inside a homogeneous human torso model with a realistic shape. The body surface ECG potentials were calculated by solving the volume conductor problem in the heart–torso model using the boundary element method (see Wei et al. [26] for details of the calculation). The 12-lead ECG was then obtained by the operation of potentials at the standard electrode positions, displayed by the red dots in Fig. 2.

Find the optimal action potential duration gradient configuration

Because the excitation sequence was the same for each simulation, the simulated secondary T wave was identical, so the simulated primary T wave was a good approximation of the T wave and vice versa. Given Gambill et al. [25] only provided data of T-wave amplitudes, the simulated T-wave amplitudes were used and compared with the clinical data.

To judge the similarity of simulated T-wave amplitudes to the clinical values, the ratio of T-wave difference to the clinical amplitude in every lead was calculated and the simulation with the least sum of the square ratios was of the optimal APD gradient configuration.

In addition to the T-wave amplitude, the interval from the peak of the T wave to the end of the T wave (Tpeak–Tend) in the V5 lead [31] was calculated as an auxiliary parameter to evaluate the similarity between simulated and clinical data.

Results

Simulation results of Models 1 and 2

The blue trace in Fig. 3 displays the simulated ECG of Model 1, namely the model with the homogeneous APD. It is obvious that the T-wave direction is opposite to the direction of the prominent part of the QRS complex in the same lead. This result agrees with the prediction of Harumi et al. [1]. Apparently, these T waves are quite different from those shown by the black traces in Fig. 3, which have amplitudes of the clinical reports.

The red trace shows the ECG generated by the simulation of Model 2. We can see that when the transmural APD gradient was added to the ventricles, the derived T-wave amplitudes were closer to the clinical values in many leads, except for the slightly expanded deviation in the aVL lead. However, apart from the V2 lead, the T-wave amplitudes of Model 2 were still considerably different from the clinical values.

Simulation results of Models 3–5

Figs. 4–6 show the T waves computed from Models 3–5 with different APD dispersions, respectively. The changing apicobasal APD gradient mainly influenced the T waves in the frontal plane leads. The changing interventricular APD gradient made noticeable changes to the T waves in most of the leads, and the changing anteroposterior APD gradient mainly affected the precordial leads. We also noticed that the respective T-wave amplitude and polarity change trends in response to the changes of these three APD gradients were quite different. Although simulations with certain APD gradients could generate T waves consistent with the clinical amplitudes in some leads, no ideal match in all leads was obtained from these models.

Simulation results of optimized combinations of gradients in different axes

Because models with a single APD gradient cannot generate T waves with amplitudes close to clinical values in all leads, we tried to simulate ECGs in models incorporating several different APD gradients.

First, we assumed that there was no APD gradient in the anteroposterior axis. By using an optimized configuration of $Gradient_T$ = 1.33 ms/mm, $Gradient_{AB}$ = 0.1987 ms/mm and $Gradient_{IV}$ = −15 ms (hereinafter referred to as Model 6), we obtained T waves shown by the blue traces in Fig. 7. These T waves did indeed show significantly improved consistency with the clinical amplitudes. In spite of this, good agreement with clinical values was only confined to the limb leads. The polarity of the T wave in the V1 lead was opposite to the clinical polarity, and the T-wave amplitudes in the V2 to V6 leads were only 32% to 67% of the corresponding clinical values (see Table 2).

We introduced the anteroposterior APD gradient into the model and found that when the ventricles had settings of $Gradient_T$ = 1.33 ms/mm, $Gradient_{AB}$ = 0.0287 ms/mm, $Gradient_{IV}$ = −22 ms and $Gradient_{AP}$ = 24 ms (hereinafter referred to as Model 7), the simulated T waves (shown by the red waveforms in Fig. 7) had the closest similarity to the clinical amplitudes. The T waves in the limb leads matched the clinical amplitudes quite well, as evidenced by the coincidences of the

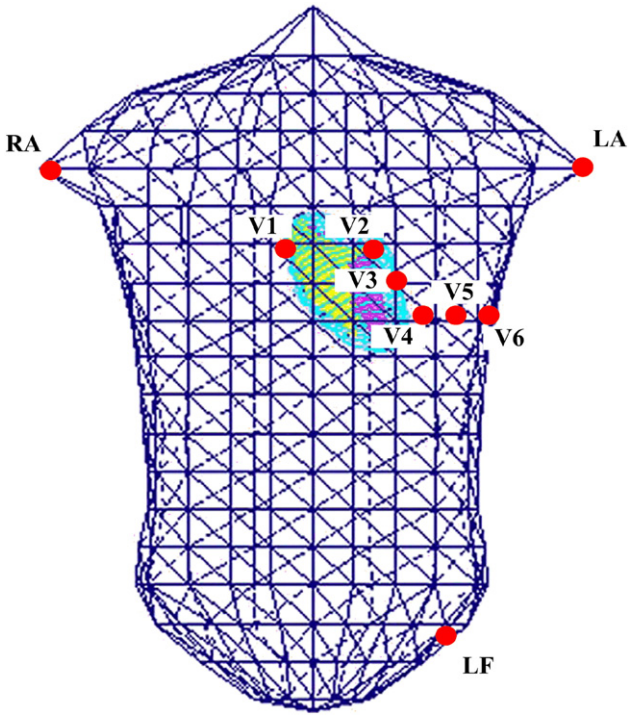

Fig. 2. The heart model inside a torso. The red dots indicate the ECG electrode locations. Key: RA = right arm, LA = left arm, LF = left foot.

red and black traces. Table 2 shows a comparison of the simulated T waves between Models 6 and 7. These percentages are ratios of the simulated T-wave amplitudes to their corresponding clinical values. Although neither Model 6 nor Model 7 exactly reproduced the clinical amplitudes of the T waves, the latter had an improved similarity. This improvement did not happen in every lead: in II, III, aVF and V4 leads, the T-wave amplitudes in Model 6 were even closer to the clinical amplitudes. However, the differences seen in these leads between the two models were relatively small, ranging from

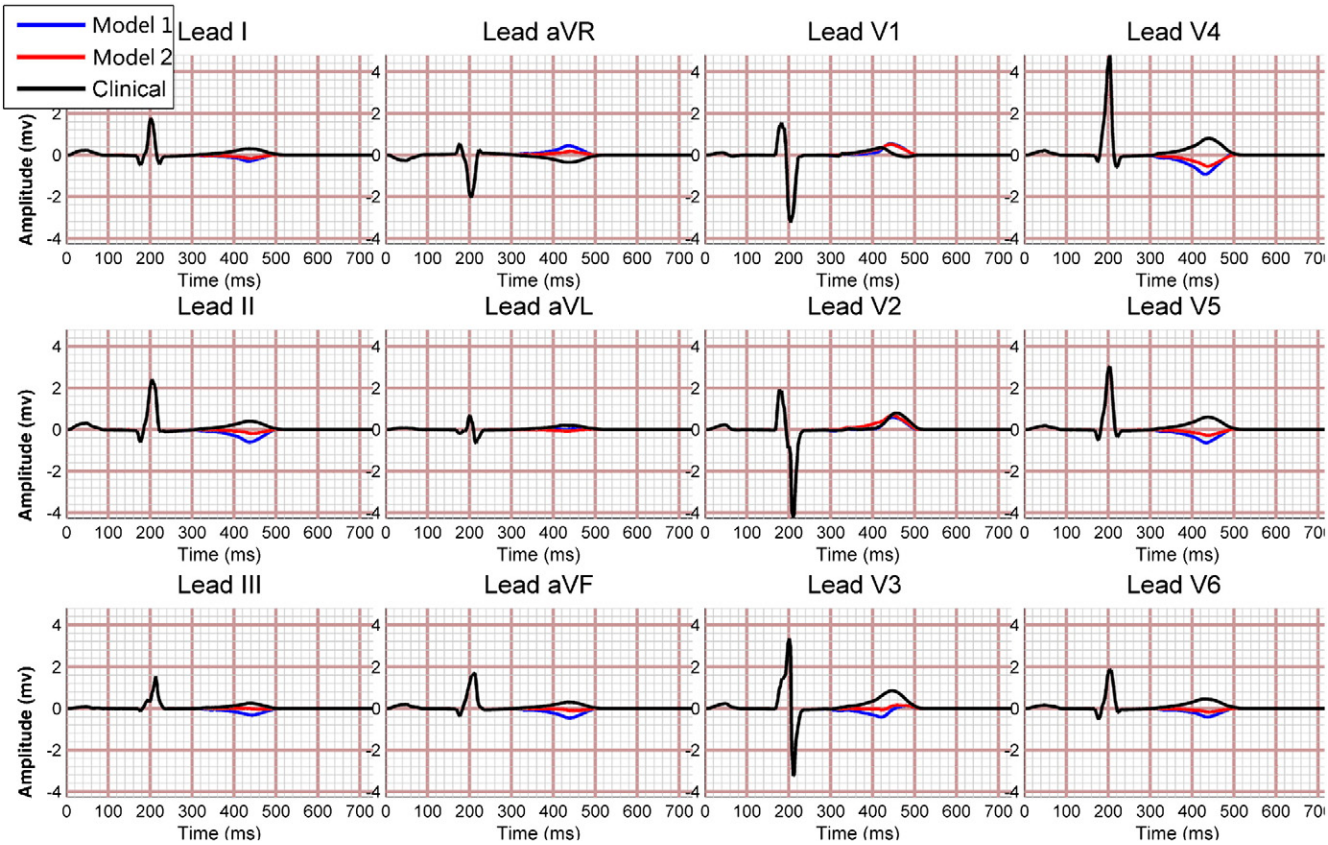

Fig. 3. The simulated ECGs using Models 1 and 2 and the clinical ECG.

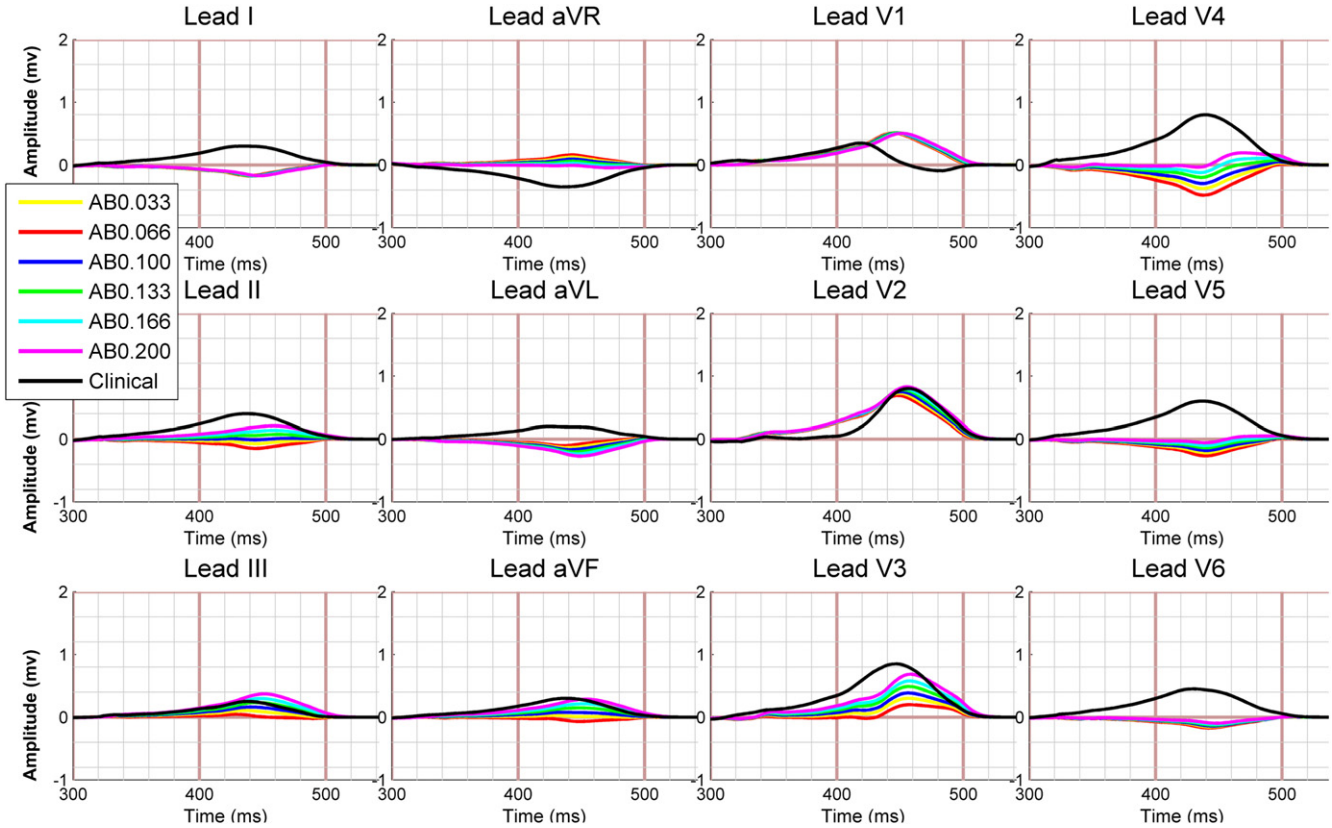

Fig. 4. The simulated T waves resulting from Model 3. The "AB" in the legend box means the apicobasal APD gradient, and the number to the right indicates the value of the APD gradient (unit: ms/mm). No close match in all leads between the simulated T wave and the clinical T wave was obtained.

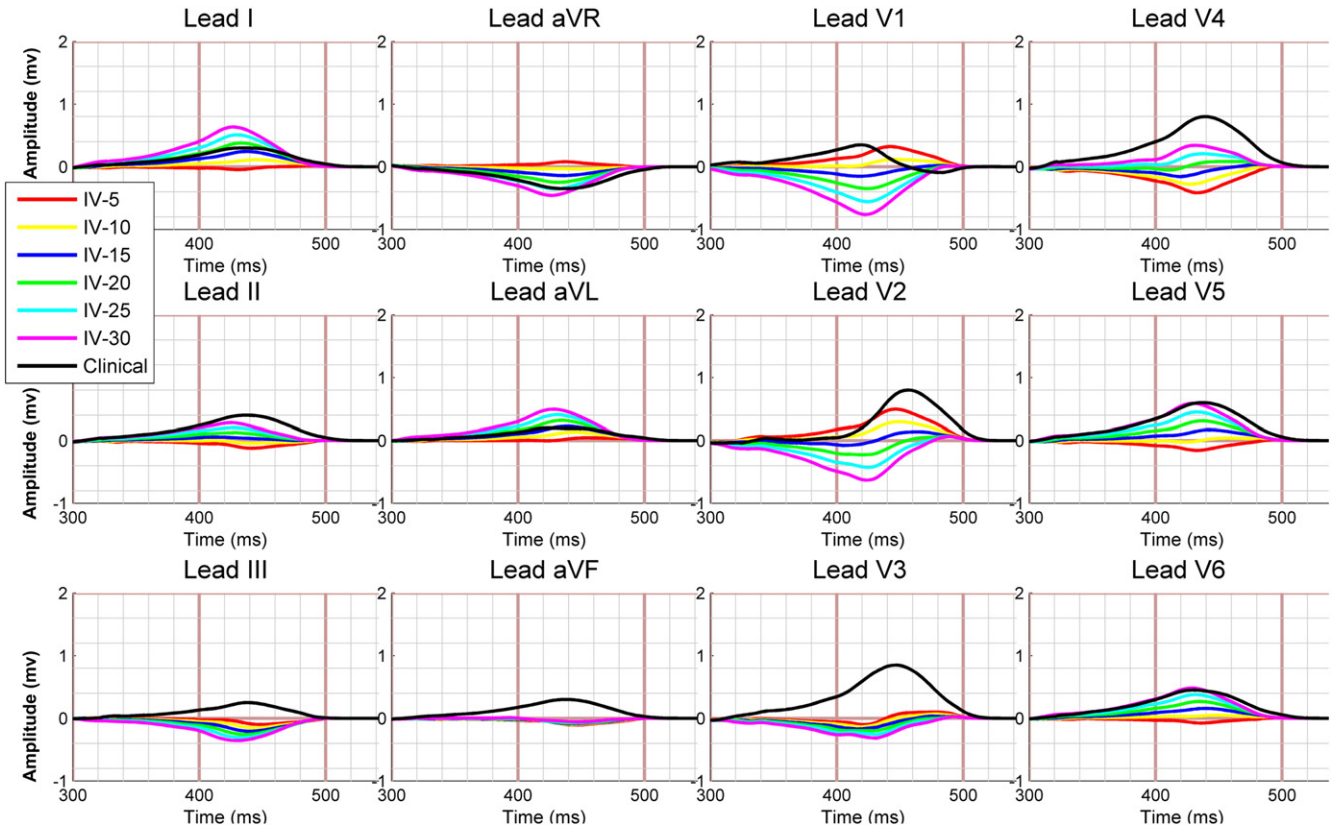

Fig. 5. The simulated T waves resulting from Model 4. The "IV" in the legend box represents the APD dispersion in the interventricular axis, and the number to the right indicates the value of the APD difference (unit: ms). No close match in all leads between the simulated T wave and the clinical T wave was obtained.

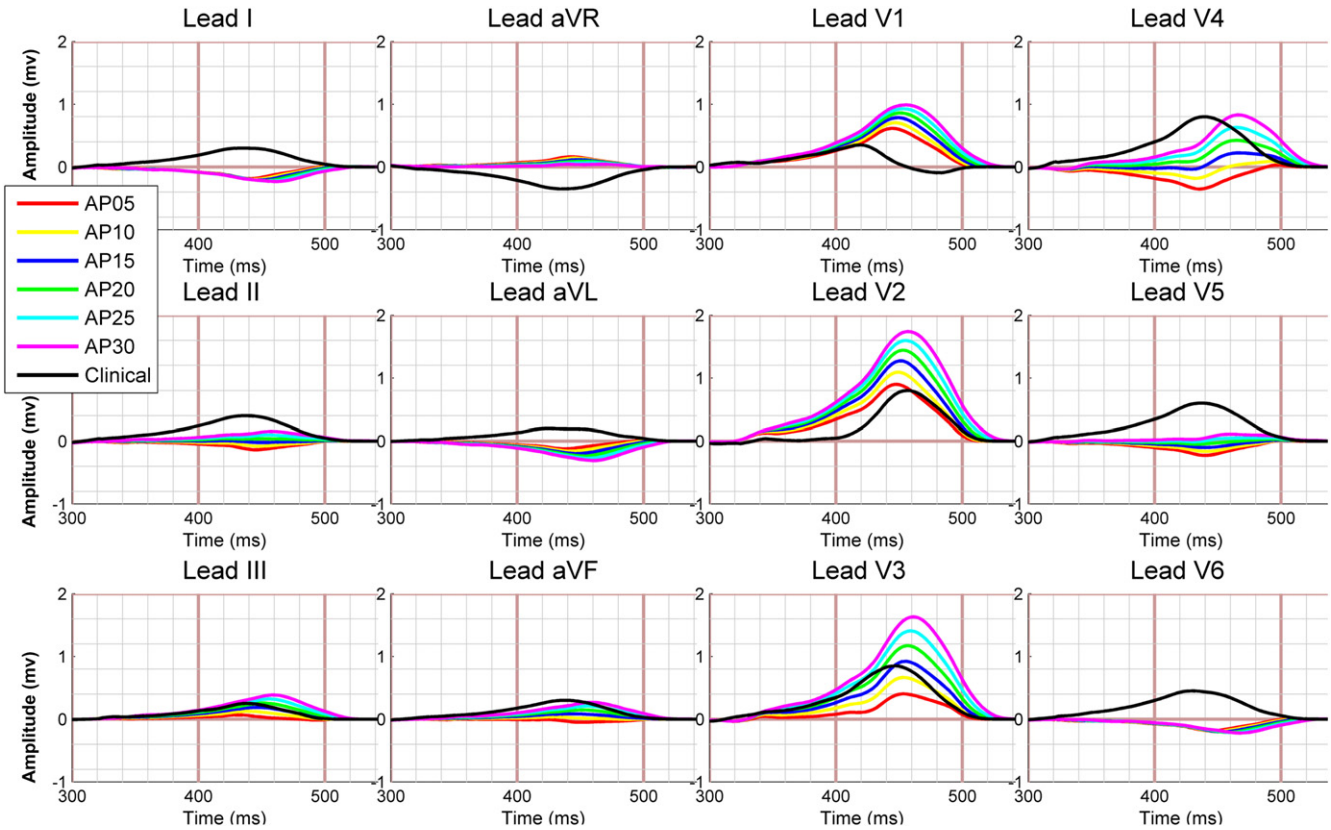

Fig. 6. The simulated T waves resulting from Model 5. The "AP" in the legend box means the APD dispersion in the anteroposterior axis, and the number to the right indicates the value of the APD difference (unit: ms). No close match in all leads between the simulated T wave and the clinical T wave was obtained.

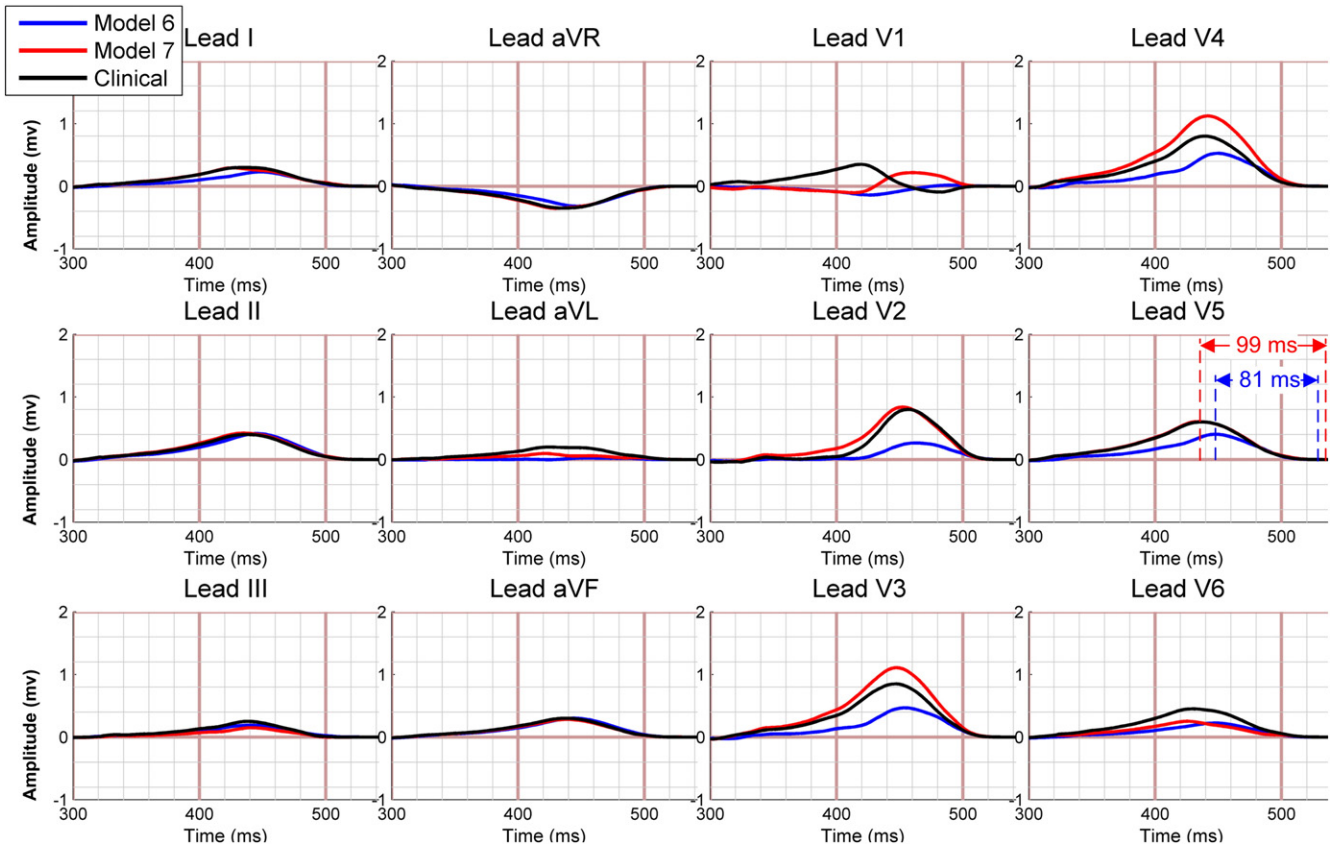

Fig. 7. The simulated T waves resulting from Models 6 and 7 and the clinical T wave. The blue and red vertical dashed lines in the V5 lead show the Tpeak-Tend of Models 6 and 7, respectively.

Table 2
The ratios of simulated T-wave amplitudes to clinical values.

Model	*I*	*II*	*III*	*aVR*	*aVL*	*aVF*
6	76.07%	103.35%	75.84%	91.63%	12.25%	100.17%
7	97.87%	104.85%	59.80%	100.91%	47.95%	94.30%
Improvement	21.80%	−1.50%	−16.04%	7.46%	35.70%	−5.57%
Model	*V1*	*V2*	*V3*	*V4*	*V5*	*V6*
6	−40.23%	32.99%	54.91%	65.80%	67.17%	49.87%
7	61.97%	104.65%	130.35%	140.34%	100.98%	55.96%
Improvement	102.2%	62.36%	14.74%	−6.14%	31.85%	6.09%

1.5% to 16.04%. In contrast, the changes in the other leads were much more pronounced, ranging from 6.09% to 102.2% with an average of 35.28%. The T-wave polarity in the V1 lead became concordant with its preceding QRS complex. This means that the direction of every T wave simulated in Model 7 matched the clinical observations. The vertical lines in Fig. 7 indicated the Tpeak–Tend of Models 6 (blue dashed lines, 81 ms) and 7 (red dashed lines, 99 ms). Fig. 8 displays the APD distribution of Model 7. The APD distribution in Model 7 was very complicated, as shown by the distinct APD variations in left–right, front–back and transmural directions.

Discussion

Transmural action potential duration gradient in the heart

Transmural APD heterogeneity was once considered to be the major cause for the T wave and QRS complex of the human ECG having the same polarity [1], but the transmural APD gradient alone cannot explain why the T wave is concordant with the QRS complex. It is known that the T wave is caused by the dispersion of repolarization [13,15]. To generate a T wave with the same polarity as the QRS complex, the epicardial cells have to repolarize earlier than the endocardial cells [1,17] and there are differences in their AP morphologies [32]. However, recent clinical studies have shown that although the transmural APD did increase gradually from the epicardium to the endocardium, the endocardium repolarized earlier than the epicardium [33] or almost simultaneously [34]. This is because the repolarization time of an individual cell is calculated by adding its APD to its depolarization time, and the transmural APD increment from the epicardium to the endocardium is not long enough to compensate for the change in the transmural activation time. The ECG simulated by Model 2 manifested discordant T waves in most of the leads. Hence, besides the transmural APD gradient, there must be other APD heterogeneities contributing to the genesis of the T wave.

The contributions of apicobasal, interventricular and anteroposterior action potential duration gradients

The apicobasal APD gradient is also recognized as one of the primary causes of T-wave concordance [6,18,35].

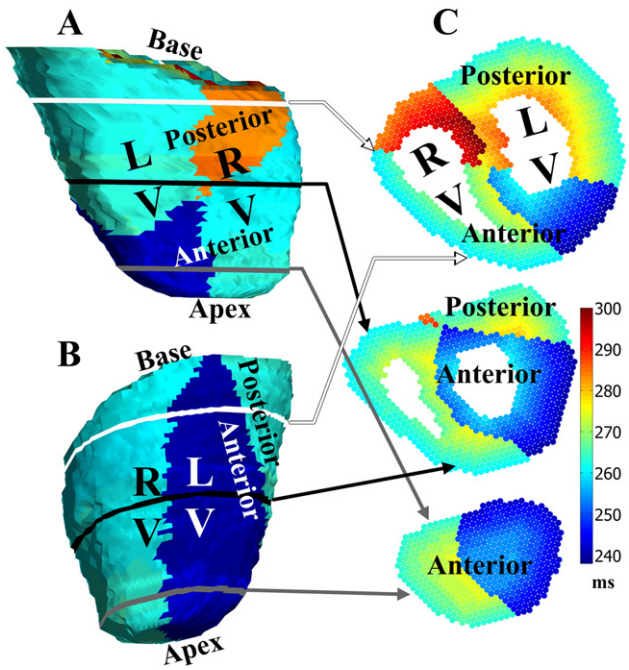

Fig. 8. The APD distribution in Model 7. (A): The APD distribution on diaphragmatic surface from a right posterior oblique view; (B): The APD distribution on sternocostal surface, seen from an LAO view; (C): Representative cross sections whose locations are indicated by the white, black and gray lines in A and B. Key: RV = right ventricle, LV = left ventricle.

However, our study demonstrated that a model with a combination of transmural and apicobasal APD gradients (Model 3) still did not generate T waves with clinically comparable amplitudes in all leads.

Because the difference between the clinical values and the amplitudes simulated in Model 2 varied among the 12 leads (e.g., the drop in the V4 lead was very large, but the drop in the V2 lead was relatively small), changing another single APD gradient (Models 3–5) could only generate T waves with amplitudes matching the clinical values in a limited number of leads. In addition, a similarity to the clinical values could never be reached in some leads, because changing the APD gradient did not always bring about desirable changes in the T-wave amplitudes. For example, in the simulations of Model 4 (Fig. 5), when the interventricular APD difference was −15 ms, the simulated T waves in the I and aVL leads showed good agreement with the clinical amplitudes; if we wanted to simulate T waves with amplitudes close to the clinical amplitudes in the aVR and V6 leads, we had to expand the interventricular APD difference to −30 ms, and this led to deviations of the simulated T waves from the clinical amplitudes in the I and aVL leads. It is obvious that changing the interventricular APD heterogeneity alone could not generate a T wave matching the clinical signal in the aVF lead, because there was little change in the T-wave amplitude in response to the change in APD heterogeneity. This dilemma existed in all of the simulations created by Models 3–5, implying that a change in a single APD gradient was not capable of reproducing a T wave with a clinical amplitude in every lead. This is in line with the findings of Weiss et al. [21].

The necessity of including the anteroposterior action potential duration gradient to simulate the clinically comparable T waves

From the simulations using Models 3–5, we noticed that the uneven amplitude changes provided by different APD gradients might be smoothed out if the changes to the APD gradients in various axes were combined. Indeed, a combination of transmural, apicobasal and interventricular APD gradients did generate ECGs with T waves closer to the clinical observations compared with the results from Models 3–5. Adding the anteroposterior APD gradient into the model provided a striking improvement in the similarities to the clinical values (see Table 2). Although there was hardly difference between the QT interval of Models 6 and 7 (363 ms vs. 366 ms), the Tpeak–Tend of Model 7 (99 ms) was much closer to the clinical data reported by Takenaka et al. (heart rate-corrected Tpeak–Tend, 99 ± 36 ms) [31] and Merri et al. (113 ms) [36] than Model 6 (81 ms). This is strong evidence that the anteroposterior APD dispersion is essential to forming the normal T wave. Thus our simulation study supports that the anteroposterior APD gradient plays an important role in the T-wave genesis.

Comparing simulation results with clinical studies

A comparison between Fig. 8 and the clinical epicardial activation recovery interval (ARI, a surrogate of APD [37]) map [38] demonstrates that, to a large extent, the APD distribution in Model 7 faithfully reproduced the clinical findings: the longest APD was at the posterior basal ventricle, and the shortest APD was at the anterior apical ventricle. The APD in the anterior RV and the posterior LV were almost the same. The endocardial and epicardial APD dispersions in Model 7 were also similar to the repolarization time dispersions found in clinical reports (8 ms vs. 14 ± 2 ms and 47 ms vs. 50 ± 9 ms, respectively) [34]. Ramanathan et al. [38] reported that the average ARI of the RV was 32 ms longer than that of the LV, and the apex-to-base APD dispersion was 30 ms. The optimal APD configuration includes an interventricular APD difference of −22 ms (longer RV APD) and an apex-to-base APD dispersion of about 26 ms (the sum of an anteroposterior difference of 24 ms and an apicobasal APD gradient of 0.0287 ms/mm multiplied by 69 mm). Thus, it is safe to conclude that the APD distribution of Model 7 was close to the clinical measurements. The consistency of the simulation results with the clinical data enhances the reliability of our study.

Limitations

The configurations of the four APD gradients used in this study were somewhat simplified. A realistic T wave is generated in a beating heart; however, our heart model did not involve the movement of cardiac muscle. The heart model was put in a homogeneous torso without other organs like lungs, but an inhomogeneous torso model can provide more precise results [39]. Our simulations only took the influence of the APD into account; however, the AP morphology may also affect the T wave [32]. We took the T-wave amplitude as the major parameter for comparison without using other measures of concordance like the spatial QRS-T angle [40] which can more objectively interpret the simulation results and determine the optimal configurations of APD gradients.

Conclusions

Our simulation results validated that the anteroposterior APD gradient is a necessary consideration in accounting for the T wave being concordant with QRS complex in the human ECG. The transmural, apicobasal, interventricular and the anteroposterior APD gradient are all essential to the genesis of the clinical T wave. The setup of the optimal APD distribution in our model simulated T waves that were very similar to the clinical findings. This study contributes to the theoretical and clinical understanding of the mechanism that generates the T wave.

Acknowledgments

We thank Dr. Weijia Lu for his valuable assistance to the study. This work is supported in part by Japan Society for the Promotion of Science under the Grants-In-Aid for Scientific Research (**No**. 24500369).

References

[1] Harumi K, Burgess MJ, Abildskov JA. A theoretic model of the T Wave. Circulation 1966;34(4):657–68.

[2] Opthof T, Coronel R, Janse MJ. Is there a significant transmural gradient in repolarization time in the intact heart?: Repolarization Gradients in the Intact Heart. Circ Arrhythm Electrophysiol 2009;2(1):89–96.

[3] Draisma HHM, Schalij MJ, van der Wall EE, Swenne CA. Elucidation of the spatial ventricular gradient and its link with dispersion of repolarization. Heart Rhythm 2006;3(9):1092–9.

[4] Abildskov JA, Burgess MJ, Millar K, Wyatt R, Baule G. The primary T wave—a new electrocardiographic waveform. Am Heart J 1971;81(2):242–9.

[5] Franz MR, Bargheer K, Rafflenbeul W, Haverich A, Lichtlen PR. Monophasic action potential mapping in human subjects with normal electrocardiograms: direct evidence for the genesis of the T wave. Circulation 1987;75(2):379–86.

[6] de Bakker JM, Opthof T. Is the apico-basal gradient larger than the transmural gradient? J Cardiovasc pharmacol 2002;39(3):328–31.

[7] Taggart P, Sutton PMI, Opthof T, Coronel R, Trimlett R, Pugsley W, et al. Transmural repolarisation in the left ventricle in humans during normoxia and ischaemia. Cardiovasc Res 2001;50(3):454–62.

[8] Nash MP, Bradley CP, Sutton PM, Clayton RH, Kallis P, Hayward MP, et al. Whole heart action potential duration restitution properties in cardiac patients: a combined clinical and modelling study. Exp Physiol 2006;91(2):339–54.

[9] Yue AM, Franz MR, Roberts PR, Morgan JM. Global Endocardial Electrical Restitution in Human Right and Left Ventricles Determined by Noncontact Mapping. J Am Coll Cardiol 2005;46(6):1067–75.

[10] Arini PD, Laciar E. Quantification of cardiac ventricular repolarization and its spatial dispersion through the surface electrocardiogram. Rev Argent Cardiol 2009;77(1):47–55.

[11] Durrer D, Van Dam RT, Freud GE, Janse MJ, Meijler FL, Arzbaecher RC. Total excitation of the isolated human heart. Circulation 1970;41(6):899–912.

[12] Patel C, Burke JF, Patel H, Gupta P, Kowey PR, Antzelevitch C, et al. Is there a significant transmural gradient in repolarization time in the intact heart?: Cellular basis of the T Wave: A century of Controversy. Circ Arrhythmia Elec 2009;2(1):80–8.

[13] Janse MJ, Coronel R, Opthof T, Sosunov EA, Anyukhovsky EP, Rosen MR. Repolarization gradients in the intact heart: Transmural or apico-basal? Prog Biophys Mol Biol 2012;109(1–2):6–15.

[14] Burdon-Sanderson J, Page FJM. On the time-relations of the excitatory process in the ventricle of the heart of the frog. J Physiol 1880;2(5–6):384–435.

[15] Yan G, Lankipalli RS, Burke JF, Musco S, Kowey PR. Ventricular Repolarization Components on the Electrocardiogram: Cellular Basis and Clinical Significance. J Am Coll Cardiol 2003;42(3):401–9.

[16] Yan G, Antzelevitch C. Cellular basis for the normal T Wave and the electrocardiographic manifestations of the long-QT syndrome. Circulation 1998;98(18):1928–36.

[17] Van Huysduynen BH, Swenne CA, Draisma HHM, Antoni ML, Van De Vooren H, Van Der Wall EE, et al. Validation of ECG Indices of ventricular repolarization heterogeneity: A computer simulation study. J Cardiovasc Electrophysiol 2005;16(10):1097–103.

[18] Xue J, Chen Y, Han X, Gao W. Electrocardiographic morphology changes with different type of repolarization dispersions. J Electrocardiol 2010;43(6):553–9.

[19] Okada J, Washio T, Maehara A, Momomura S, Sugiura S, Hisada T. Transmural and apicobasal gradients in repolarization contribute to T-wave genesis in human surface ECG. Am J Physiol Heart C 2011;301(1):H200–8.

[20] Okada J, Sasaki T, Washio T, Yamashita H, Kariya T, Imai Y, et al. Patient specific simulation of body surface ECG using the finite element method. PACE 2013;36(3):309–21.

[21] Weiss DL, Seemann G, Keller DUJ, Farina D, Sachse FB, Dossel O. Modeling of heterogeneous electrophysiology in the human heart with respect to ECG genesis. Proceedings of computers in cardiology. Durham, NC: IEEE Computer Society Press; 2007. p. 49–52.

[22] Keller DUJ, Weiss DL, Doessel O, Seemann G. Influence of I_{Ks} heterogeneities on the genesis of the T-wave: A computational evaluation. IEEE T Biomed Eng 2012;59(2):311–22.

[23] Meijborg VMF, Conrath CE, Opthof T, Belterman CNW, de Bakker JMT, Coronel R. Electrocardiographic T Wave and its Relation With Ventricular Repolarization Along Major Anatomical Axes. Circ Arrhythmia Elec 2014;7(3):524–31.

[24] Arteyeva NV, Azarov JE, Vityazev VA, Shmakov DN. Action potential duration gradients in the heart ventricles and the cardiac electric field during ventricular repolarization (a model study). J Electrocardiol 2015;48(4):678–85.

[25] Gambill CL, Wilkins ML, Haisty WK, Anderson ST, Maynard C, Wagner NB, et al. T wave amplitudes in normal populations: variation with ECG lead, sex, and age. J Electrocardiol 1995;28(3):191–7.

[26] Wei D, Okazaki O, Harumi K, Harasawa E, Hosaka H. Comparative simulation of excitation and body surface electrocardiogram with isotropic and anisotropic computer heart models. IEEE T Biomed Eng 1995;42(4):343–57.

[27] Keldermann RH, ten Tusscher KHWJ, Nash MP, Bradley CP, Hren R, Taggart P, et al. A computational study of mother rotor VF in the human ventricles. Am J Physiol Heart C 2009;296(2):H370–9.

[28] Zheng Y, Wei D, Zhu X, Chen W, Fukuda K, Shimokawa H. Ventricular fibrillation mechanisms and cardiac restitutions: An investigation by simulation study on whole-heart model. Comput Biol Med 2015;63:261–8.

[29] Zhu X, Wei D, Okazaki O. Computer simulation of clinical electrophysiological study. PACE 2012;35(6):718–29.

[30] Watanabe T, Yamaki M, Yamauchi S, Minamihaba O, Miyashita T, Kubota I, et al. Regional prolongation of ARI and altered restitution properties cause ventricular arrhythmia in heart failure. Am J Physiol Heart Circ Physiol 2002;282(1):H212–8.

[31] Merri M, Benhorin J, Alberti M, Locati E, Moss AJ. Electrocardiographic quantitation of ventricular repolarization. Circulation 1989;80(5):1301–8.

[32] Galeotti L, van Dam PM, Johannesen L, Vicente J, Strauss DG. Computer simulations to investigate the causes of T-wave notching. J Electrocardiol 2015;48(6):927–32.

[33] Conrath CE, Wilders R, Coronel R, BJ de, Taggart P, GJ de, et al. Intercellular coupling through gap junctions masks M cells in the human heart. Cardiovasc Res 2004;62(2):407–14.

[34] Chauhan VS, Downar E, Nanthakumar K, Parker JD, Ross HJ, Chan W, et al. Increased ventricular repolarization heterogeneity in patients with ventricular arrhythmia vulnerability and cardiomyopathy: a human in vivo study. Am J Physiol Heart C 2006;290(1):H79–86.

[35] Perotti LE, Krishnamoorthi S, Borgstrom NP, Ennis DB, Klug WS. Regional segmentation of ventricular models to achieve repolarization dispersion in cardiac electrophysiology modeling. Int J Numer Method Biomed Eng 2015;31(8)e2718.

[36] Takenaka K, Ai T, Shimizu W, Kobori A, Ninomiya T, Otani H, et al. Exercise stress test amplifies genotype–phenotype correlation in the LQT1 and LQT2 forms of the long-QT syndrome. Circulation 2003;107(6):838–44.

[37] Haws CW, Lux RL. Correlation between in vivo transmembrane action potential durations and activation-recovery intervals from electrograms. Effects of interventions that alter repolarization time. Circulation 1990;81(1):281–8.

[38] Ramanathan C, Jia P, Ghanem R, Ryu K, Rudy Y. Activation and repolarization of the normal human heart under complete physiological conditions. Proc Natl Acad Sci 2006;103(16):6309–14.

[39] Bradley CP, Pullan AJ, Hunter PJ. Effects of material properties and geometry on electrocardiographic forward simulations. Ann Biomed Eng 2000;28(7):721–41.

[40] Wilson FN, Macleod AG, Barker PS, Johnston FD. The determination and the significance of the areas of the ventricular deflections of the electrocardiogram. Am Heart J 1934;10(1):46–61.